Support information for:

A single-ion-conducting lithium-based montmorillonite interfacial layer for stable lithium-metal batteries

*Ting Zeng, Yu Yan, Miao He, Dayue Du, Xiaojuan Wen, Bo Zhou and Chaozhu Shu**

College of Materials and Chemistry & Chemical Engineering, Chengdu University of Technology, 1#, Dongsanlu, Erxianqiao, Chengdu 610059, Sichuan, P. R. China

**E-mail: czshu@imr.ac.cn; shuchaozhu13@cdut.edu.cn (Chaozhu Shu).*

1. Experimental section

Synthesis of Li-MMT: Li-MMT is prepared via ion exchange process[1]. MMT is dispersed into LiCl solution with vigorous stirring. Li-MMT is obtained using high-speed centrifuge and washed with deionized H_2O until Cl^- ions are complrtely removed as indicated by $AgNO_3$ test. Li-MMT samples are dried in vacuum oven for 24 hours and are grinded.

Fabrication of Artificial Li-MMT Protective Layer: 0.24 g Li-MMT powders and 0.03 g PVDF are dispersed in NMP solvent. After that, the dispersion is doctor bladed on Cu foil followed by drying at 60 °C overnight.

Material characterization: X-ray diffraction (XRD) patterns are recorded by using D/MAX-IIIC (Japan) with Cu Kα radiation with scanning range from 5° to 80°. High-resolution transmission electron microscope (HRTEM) images are recorded by FEI Tecnai G2. Scanning electron microscopy (SEM) images are recorded by using a ZEISS Gemini 300, and energy dispersive X-ray spectroscopy (EDS) analysis are conducted by Xplore 30.

Electrochemical measurements: Li|Li and Li|Cu cells are assembled in an argon-filled glove box (H_2O< 0.1 ppm, O_2< 0.1 ppm) with 1 M lithiumbis(trifluoromethanesulfonyl)imide (LiTFSI) in 1,3-dioxolane (DOL)/1,2-dimethoxyethane (DME) (1:1 w/w) as electrolyte and Celgard 2400 as separator. Each cell contains ~30 μL electrolyte. Galvanostatic discharge/charge measurements are conducted on Wuhan LAND battery testing system (CT2001A). A certain amount of Li is deposited onto the current collectors and then charged to 1.0 V (vs Li/Li^+) to

strip the Li for each cycle, during which the Coulombic efficiency (CE) are calculated. Nucleation overpotential is obtained from the galvanostatic discharge curves at a current density of 0.5 mA cm^{-2}. To evaluate the cycling stability, 5 mA h cm^{-2} Li is first pre-deposited on the current collectors at 0.5 mA cm^{-2}. After that, 0.5 mA h cm^{-2} Li is stripped from the deposited Li and then plated to Li-MMT-Cu@Li, Cu@Li electrodes at 0.5 mA cm^{-2}. Li-O_2 batteries are also assembled in the argon-filled glove box by employing Li-MMT-Cu@Li as anode and Super P as cathode, glass fiber (Whatman, GF/D) as the separator, 1 M LiTFSI in TEGDME solution as electrolyte. The electrochemical impedance spectroscopy (EIS) is carried out on electrochemical workstation (Bio-Logic SP-150) with a voltage amplitude of 10 mV at a frequency range of 0.01-100 kHZ. The cyclic voltammetry (CV) test is performed on Li|Cu cells using Li as counter/reference electrode in the potential range of -0.1 V~ 0.5 V at a scan rate of 5.0 mV s^{-1}. The linear sweep voltammety (LSV) test is measured using Li-MMT-Cu@stainless steel (SS) and bare Cu@SS electrodes at a scan rate of 5.0 mV s^{-1}.

Energy density: The energy density E (Wh kg^{-1}) can be obtained according to the following equations:

$$E = \frac{C \times V \times 1000}{m}$$

where V is the average discharge voltage (V), m is the total mass loading of the anode and the cathode, and C is the discharge capacity (Ah).

When the mass loading of the anode is 1 mg for Li-MMT-Cu@Li electrodes and 18 mg for bare Li electrodes, and the mass loading of the cathode remained the same, i.e.,

1 mg, the energy density of LOBs with Li-MMT-Cu@Li electrodes and bare Li electrodes was calculated as follows, respectively:

$$E_{\text{Li - MMT - Cu@Li } electrodes} = \frac{4.09210 \times 0.8 \times 1000}{2} = 1636.84 \text{ Wh kg}^{-1}$$

$$E_{\text{Bare Li electrodes}} = \frac{12.50990 \times 0.8 \times 1000}{19} = 526.73 \text{ Wh kg}^{-1}$$

2. Supporting Results and Figures

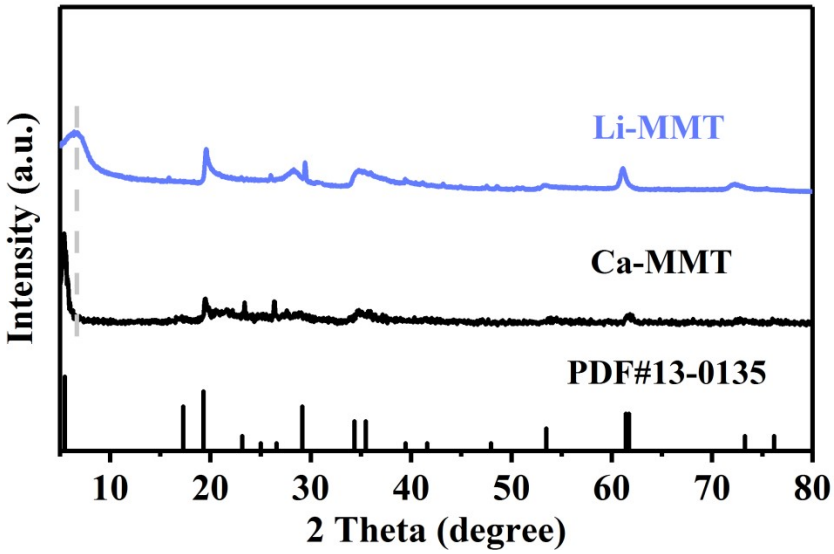

Figure S1. XRD patterns of Ca-MMT and Li-MMT.

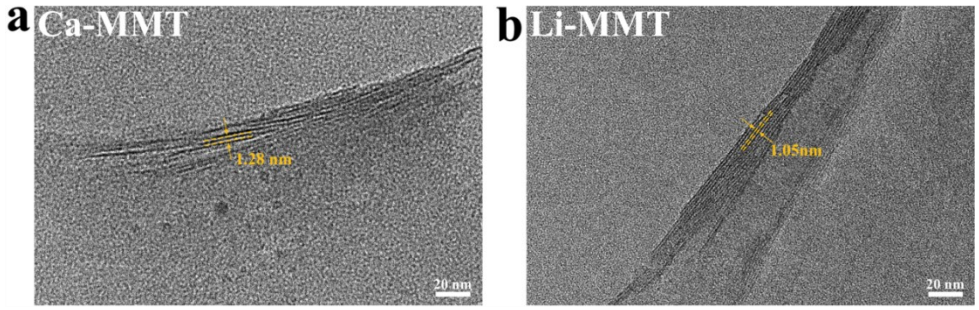

Figure S2. HRTEM images of Ca-MMT and Li-MMT.

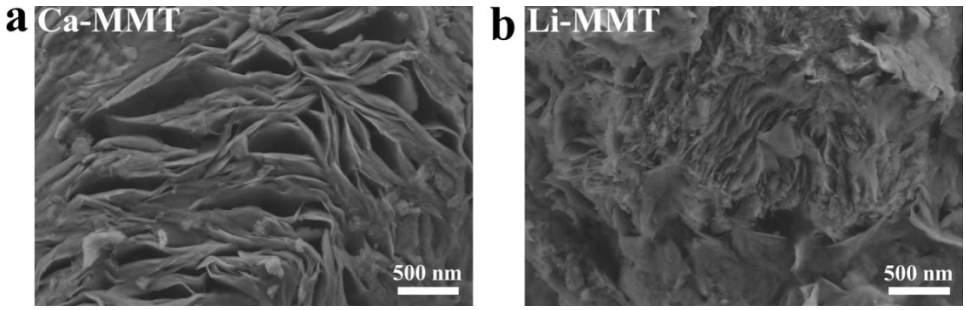

Figure S3. SEM images of Ca-MMT and Li-MMT.

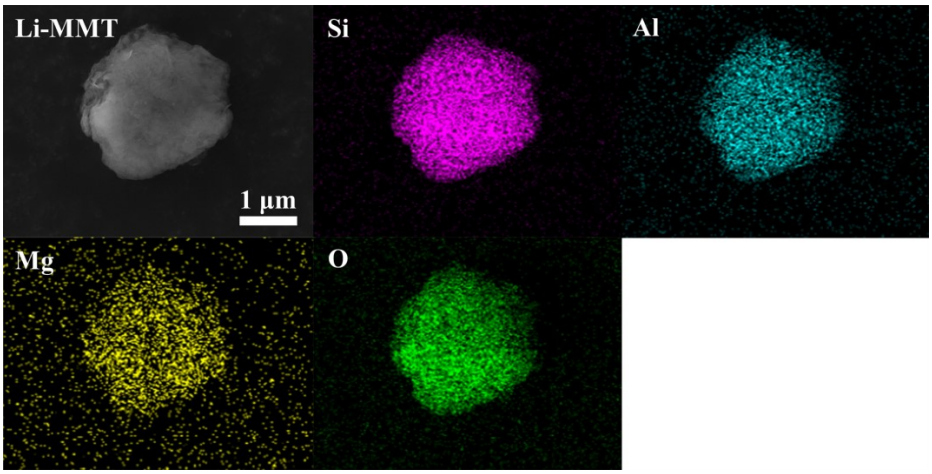

Figure S4. EDS elemental mapping images of Li-MMT.

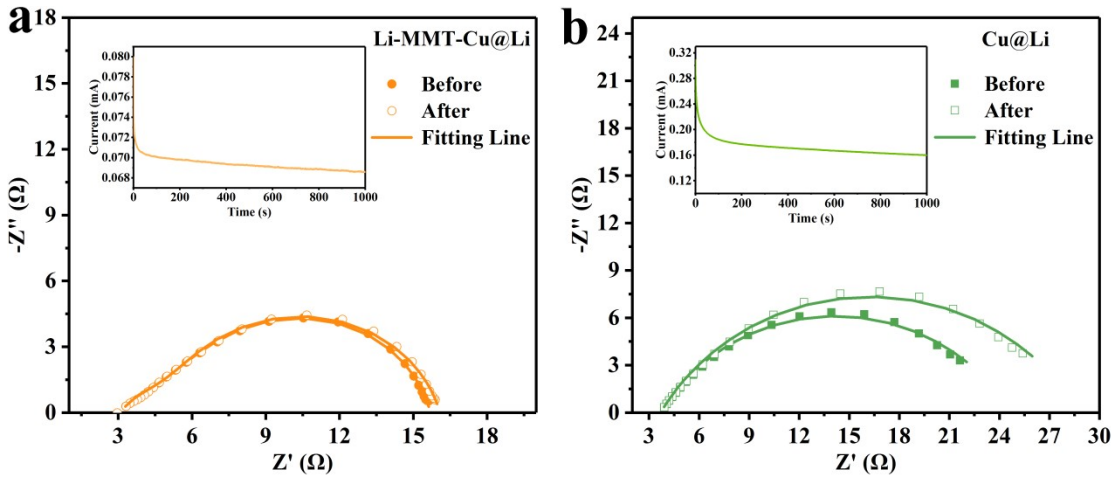

Figure S5. Nyquist plots of (a) Li-MMT-Cu@Li and (b) Cu@Li symmetric cells before/after polarization. The inset is the chronoamperogram of different symmetric cells with an applied voltage of 10 mV.

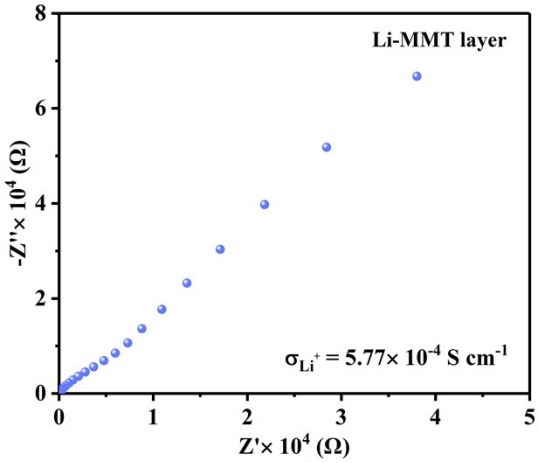

Figure S6. Nyquist plot of Li-MMT@SS|SS cells and the corresponding ionic conductivity.

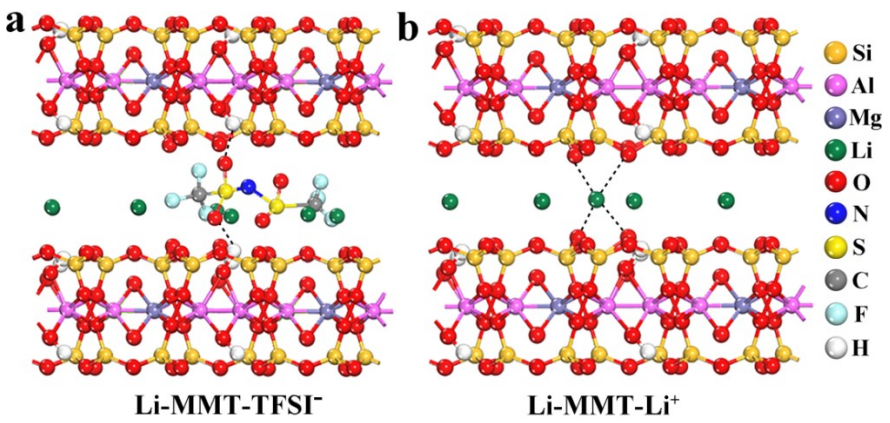

Figure S7. The adsorption configurations of Li-MMT-$TFSI^-$ and Li-MMT-Li^+ for density function theory (DFT) calculations.

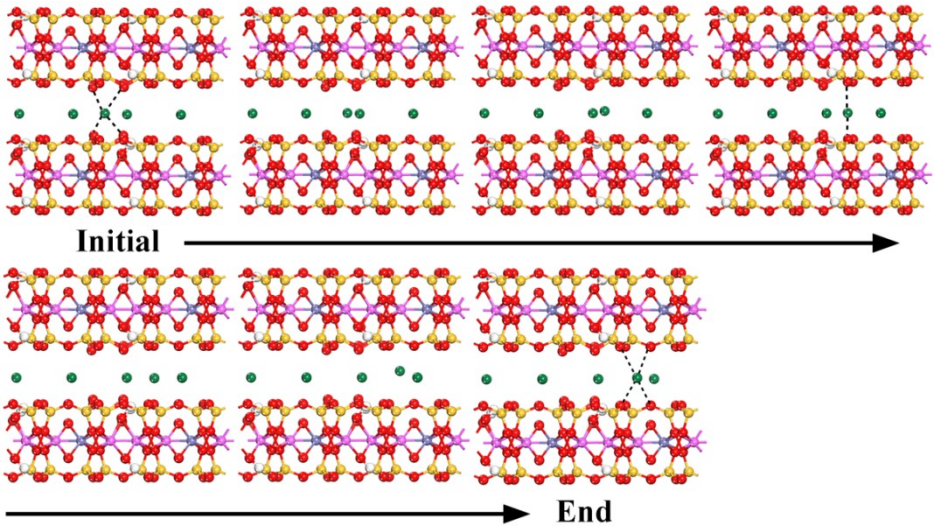

Figure S8. The specific migration pathway of Li^+ ions

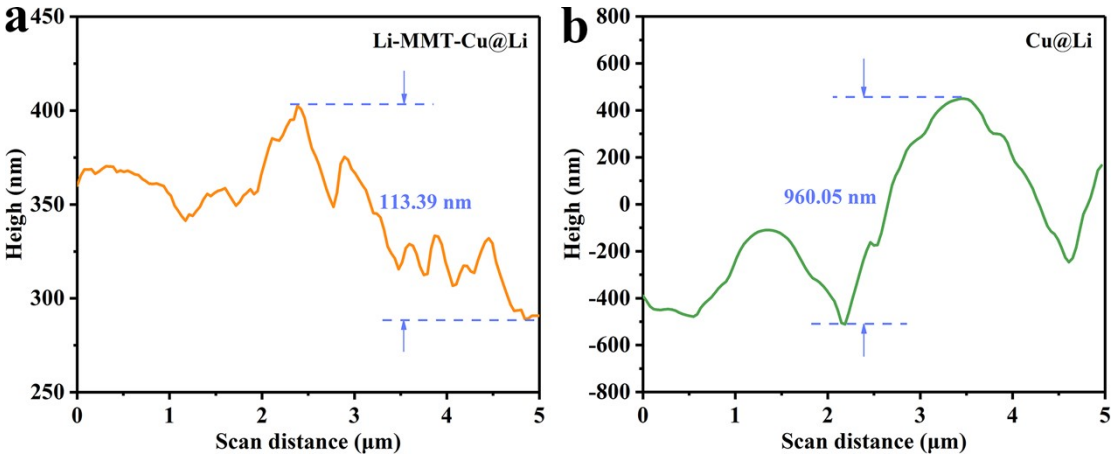

Figure S9. The height curves in AFM topography images of the surface of (a) Li-MMT-Cu@Li electrodes and (b) Cu@Li electrodes after plating 5 mAh cm^{-2} Li.

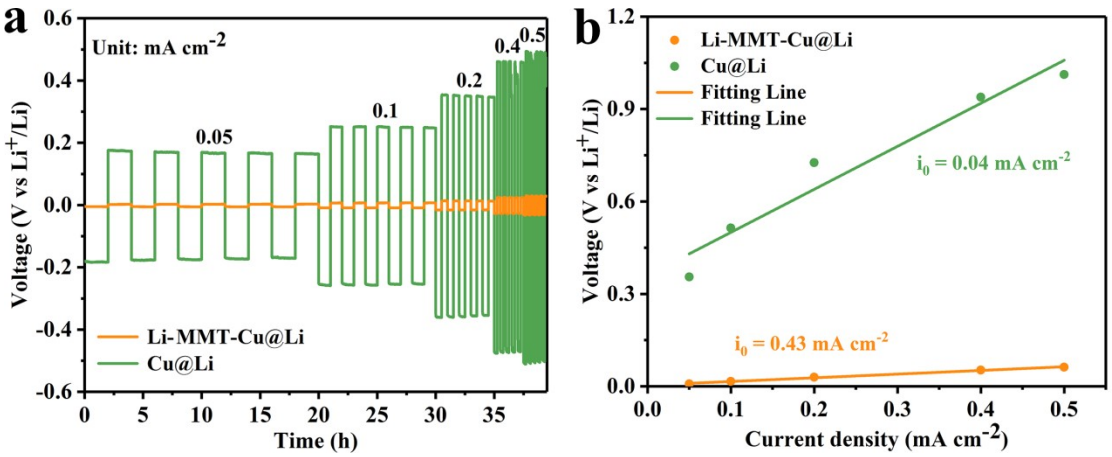

Figure S10. (a) Galvanostatic discharge/charge under different current density from 0.05 to 0.5 mA cm^{-2} with a fixed areal capacity of 0.1 mAh cm^{-2} and (b) the corresponding exchange current density.

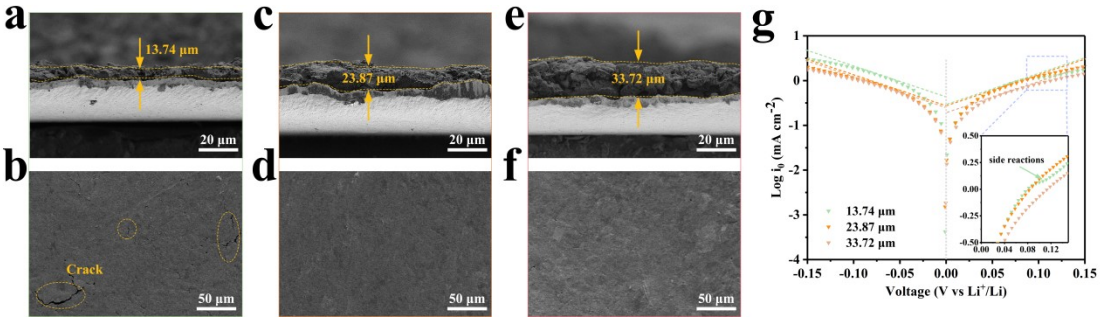

Figure S11. Cross-sectional SEM images of Li-MMT layer with different thickness of (a) 13.74 μm, (c) 23.87 μm and (e) 33.72 μm. Top-view SEM images of Li-MMT-Cu@Li electrodes with (b) 13.74 μm, (d) 23.87 μm and (f) 33.72 μm after depositing 5 mAh cm^{-2} Li under 0.5 mA cm^{-2}. (g) Tafel curves of Li|Li symmetric cells.

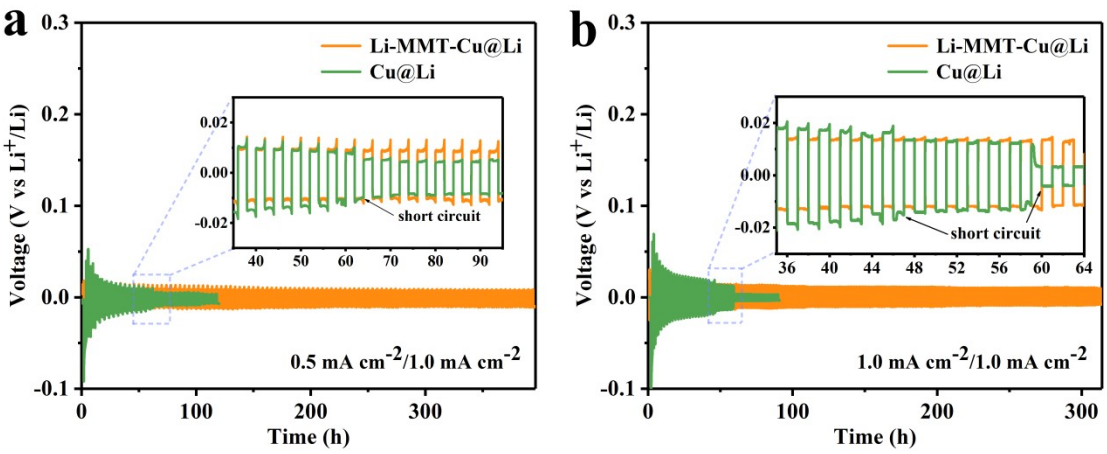

Figure S12. Long-term cycling and voltage profiles of Li|Li symmetric cells with Cu@Li and Li-MMT-Cu@Li electrodes at (a) 0.5 mA cm^{-2}/1.0 mAh cm^{-2} and (b) 1.0 mA cm^{-2}/1.0 mAh cm^{-2}. The inset is the magnified voltage profiles at selected cycles.

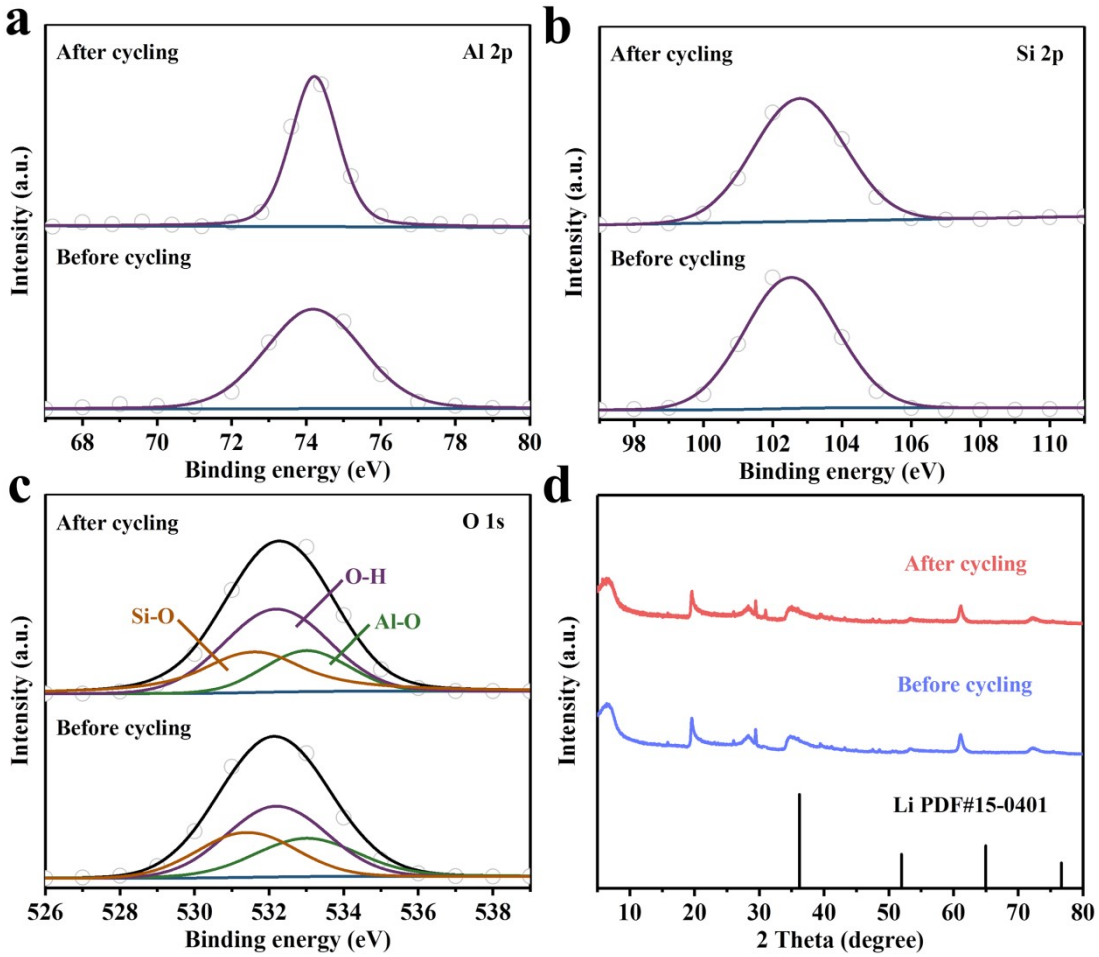

Figure S13. XPS spectra of (a) Al 2p, (b) Si 2p and (c) O 1s in the Li-MMT protective

layer before and after 50 cycles. (d) XRD patterns of the Li-MMT protective layer before and after 50 cycles.

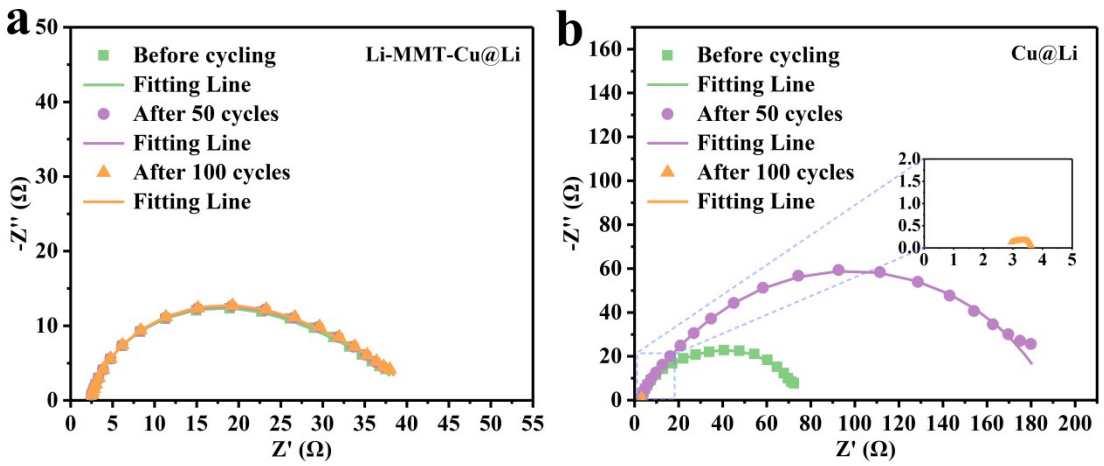

Figure S14. Electrochemical impedance spectroscopy of Li|Li symmetric cells with (a) Li-MMT-Cu@Li and (b) Cu@Li electrodes before (i.e., static placing for 1 day before testing) and after 50 cycles and 100 cycles.

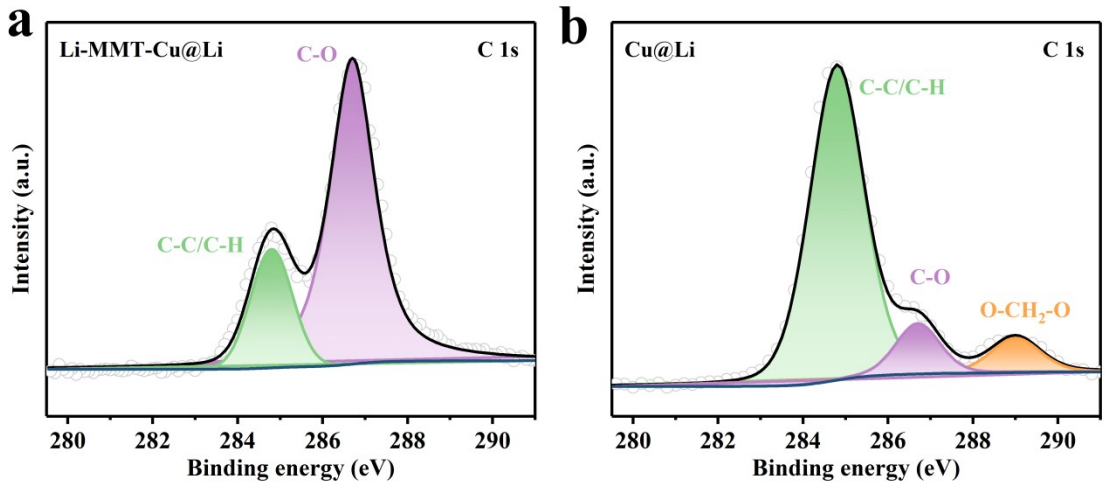

Figure S15. C 1s XPS spectra of the surface of (a) Li-MMT-Cu@Li electrodes and (b) Cu@Li electrodes after depositing 5 mAh cm^{-2} Li.

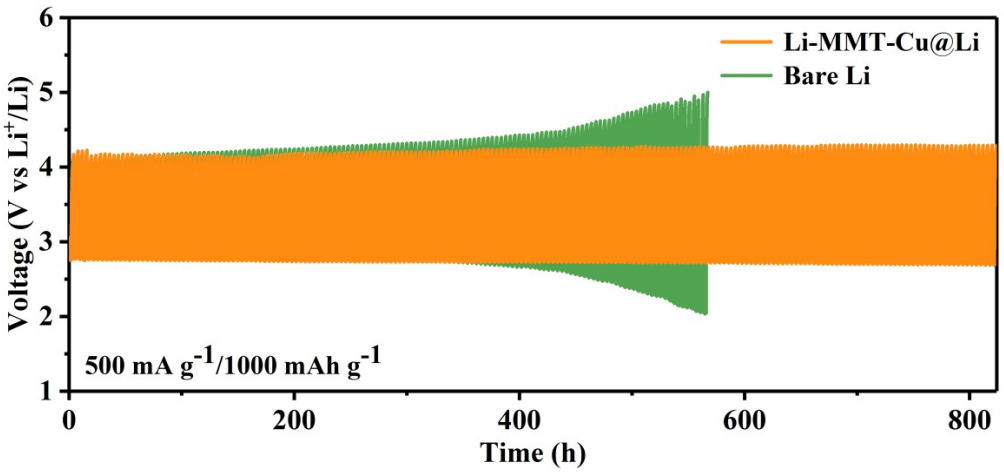

Figure S16. Cycle performance of both electrodes with a cutoff capacity of 1000 mAh g^{-1} at a current density of 500 mA g^{-1}.

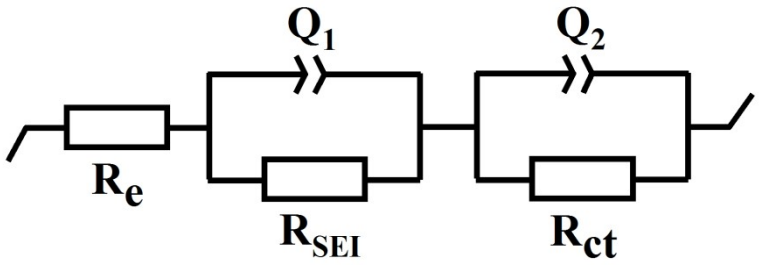

Figure S17. Equivalent circuit of the electrochemical impedance spectroscopy.

Supplementary Table 1. Fitting results of both electrodes with and without Li-MMT layer before (i.e., static placing for 2 hours) and after 50 cycles at 0.5 mA cm^{-2} and 0.5 mAh cm^{-2}.

		Before cycling (static placing for 2 hours)	After cycling
Li-MMT-Cu@Li electrodes	R_{SEI}	0.42	0.44
	R_{ct}	13.15	11.64
Cu@Li electrodes	R_{SEI}	6.09	26.99
	R_{ct}	56.08	195.30

Supplementary Table 2. Fitting results of both electrodes with and without Li-MMT layer before (i.e., static placing for 1 day) and after 50 cycles and 100 cycles at 0.5 mA cm^{-2} and 0.5 mAh cm^{-2}.

		Before cycling (static placing for 1 day)	After 50 cycles	After 100 cycles
Li-MMT-Cu@Li electrodes	R_{SEI}	12.96	13.10	13.12
	R_{ct}	24.69	24.46	24.45
Cu@Li electrodes	R_{SEI}	61.75	183.70	0.46
	R_{ct}	11.56	3.77	0.35

Supplementary Table 3. The comparison of the electrochemical performances between our work and other reported works.

Strategy	Current density (mA cm^{-2})	Areal capacity (mAh cm^{-2})	Overpotential (mV)	Cycle number (n)	Reference
PDA host	0.1	0.2	~50	200	Ref. [2]
MXene host	0.5	0.5	~25	175	Ref. [3]
Vo-TiO_2/$Ti_3C_2T_x$ host	0.1	0.1	19	350	Ref. [4]
5% Lithium nitrate	0.5	0.5	52	150	Ref. [5]
20 mM Boric acid	0.25	0.5	~80	215	Ref. [6]
0.1 M LiDFP and 0.4 M LiBOB	0.5	0.5	~50	140	Ref. [7]
Artificial dual SEI	0.5	0.5	12	200	Ref. [8]
PVDF-HFP film	0.5	0.5	~48	250	Ref. [9]
Li-MMT layer	0.5	0.5	10	650	This work

Reference

[1] Kim, S., et al., Preparation and ion-conducting behaviors of poly (ethylene oxide)-composite electrolytes containing lithium montmorillonite. Solid State Ionics, 2007, 178(13-14): 973-979.

[2] He, Y., et al., Polydopamine coating layer modified current collector for dendrite-free Li metal anode. Energy Storage Materials, 2019, 23: 418-426.

[3] Wei, C. L., et al., Isotropic Li nucleation and growth achieved by an amorphous liquid metal nucleation seed on MXene framework for dendrite-free Li metal anode. Energy Storage Materials, 2020, 26: 223-233.

[4] Yan, Y., et al., Long-cycling lithium-oxygen batteries enabled by tailoring Li nucleation and deposition via lithiophilic oxygen vacancy in Vo-TiO_2/$Ti_3C_2T_x$ composite anodes. Journal of Energy Chemistry, 2022, 65: 654-665.

[5] Tan, S. J., et al., Nitriding-interface-regulated lithium plating enables flame-retardant electrolytes for high-voltage lithium metal batteries. Angewandte Chemie International Edition, 2019, 131(23): 7884-7889.

[6] Huang, Z. M., et al., Protecting the Li-metal anode in a Li-O_2 battery by using boric acid as an SEI-forming additive. Advanced Materials, 2018, 30(39): 1803270.

[7] Zheng, H., et al., Lithium difluorophosphate-based dual-salt low concentration electrolytes for lithium metal batteries. Advanced Energy Materials, 2020, 10(30): 2001440.

[8] Guo, W., et al., Artificial dual solid-electrolyte interfaces based on in situ organothiol transformation in lithium sulfur battery. Nature communications,

2021, 12(1): 1-13.

[9] Xiao, Y., et al., Waterproof lithium metal anode enabled by cross-linking encapsulation. Science Bulletin, 2020, 65(11): 909-916.